Electronic Supplementary Information

Restructuring multi-phase interfaces from Cu-based metal-organic frameworks for selective electroreduction of CO_2 to C_2H_4

Jiye Feng,[a] Wenbiao Zhang,[a,b] Danni Shi,[a] Yingshuai Jia,[b] Yi Tang,[b] Yuying Meng,[a] and Qingsheng Gao*[a]

[a] College of Chemistry and Materials Science, Guangdong Provincial Key Laboratory of Functional Supramolecular Coordination Materials and Applications, Jinan University, Guangzhou 510632, P. R. China. E-mail: tqsgao@jnu.edu.cn

[b] Department of Chemistry, Shanghai Key Laboratory of Molecular Catalysis and Innovative Materials, Laboratory of Advanced Materials and Collaborative Innovation Center of Chemistry for Energy Materials, Fudan University, Shanghai 200433, China.

Figures and Tables

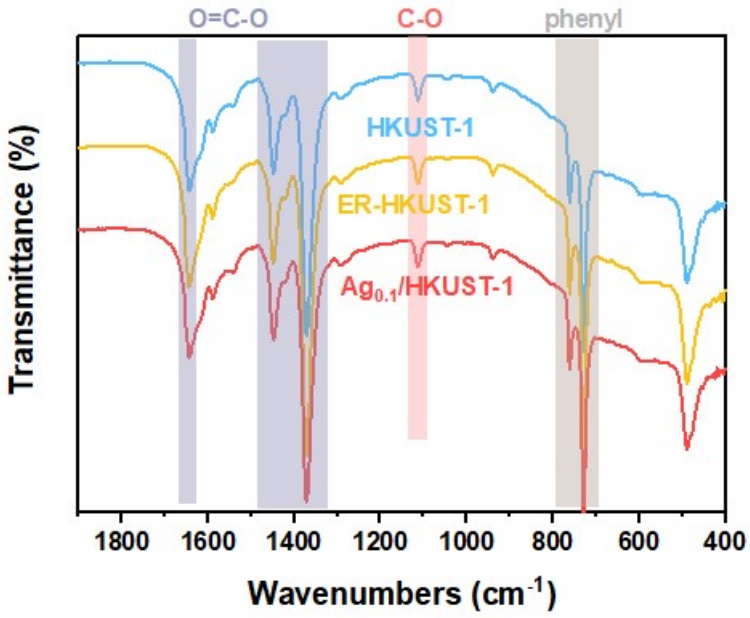

Fig. S1. FT-IR spectra of HKUST-1, ER-HKUST-1 and $Ag_{0.1}$/HKUST-1.

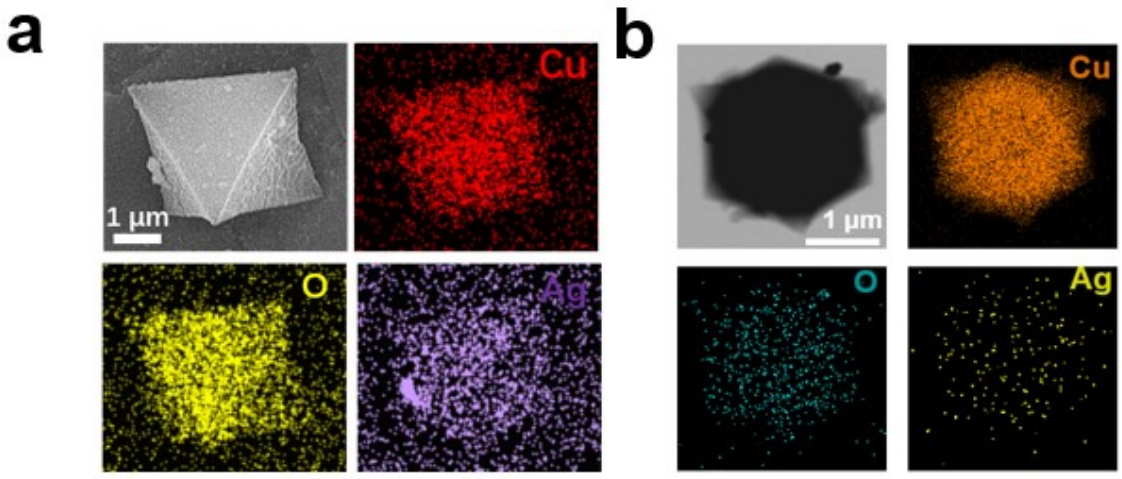

Fig. S2. (a) SEM and (b) TEM corresponding elemental mapping of $Ag_{0.1}$/HKUST-1.

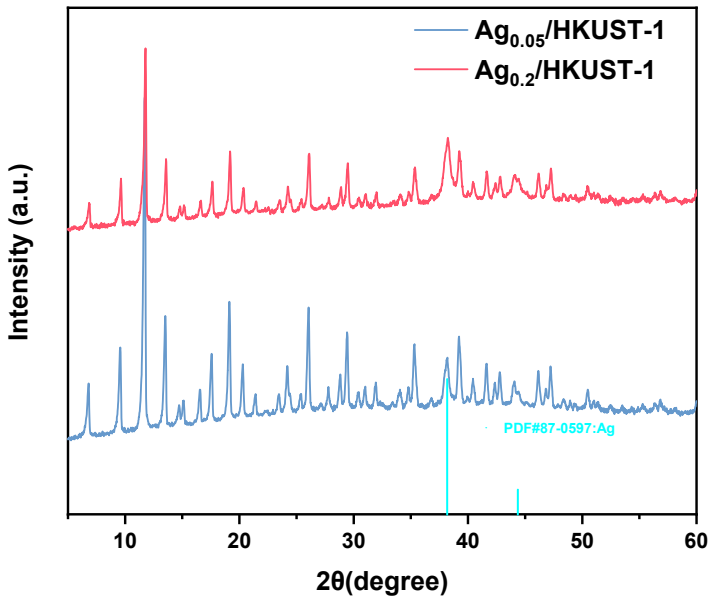

Fig. S3. XRD patterns of the $Ag_{0.05}$/HKUST-1 and $Ag_{0.2}$/HKUST-1.

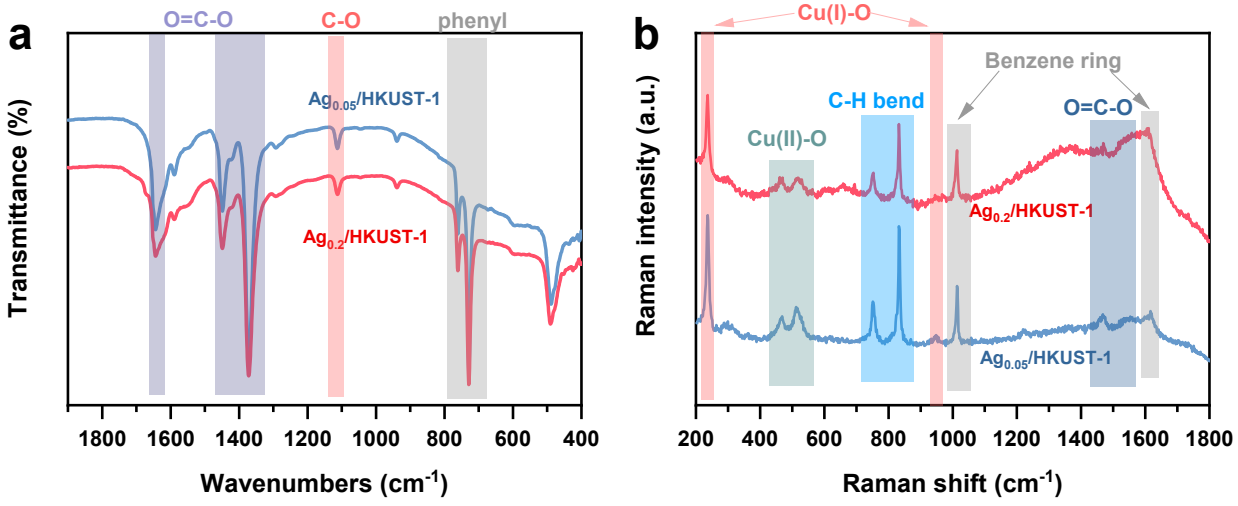

Fig. S4. (a) FT-IR spectra and (b) Raman spectra of $Ag_{0.05}$/HKUST-1 and $Ag_{0.2}$/HKUST-1.

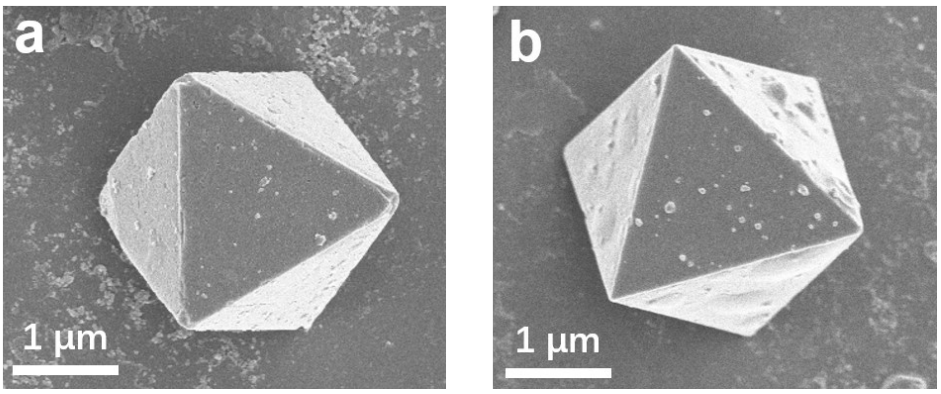

Fig. S5. SEM images of (a) $Ag_{0.05}$/HKUST-1 and (b) $Ag_{0.2}$/HKUST-1.

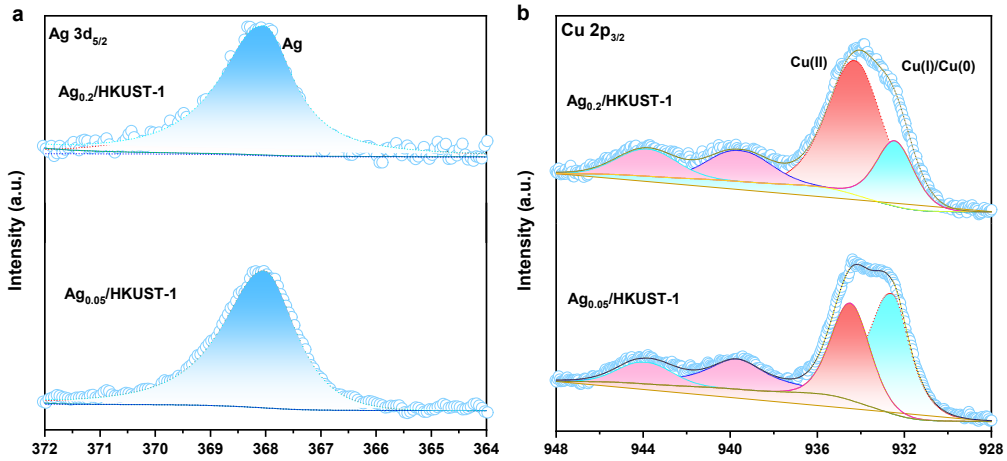

Fig. S6. High-resolution (a) Ag $3d_{5/2}$ and (b) Cu $2p_{3/2}$ XPS spectra of $Ag_{0.05}$/HKUST-1 and $Ag_{0.2}$/HKUST-1.

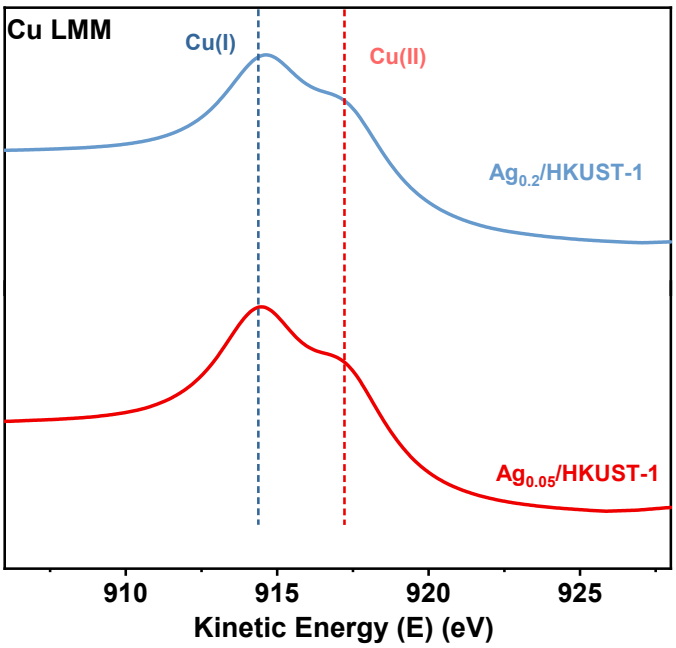

Fig. S7. Cu LMM Auger profiles of $Ag_{0.05}$/HKUST-1 and $Ag_{0.2}$/HKUST-1.

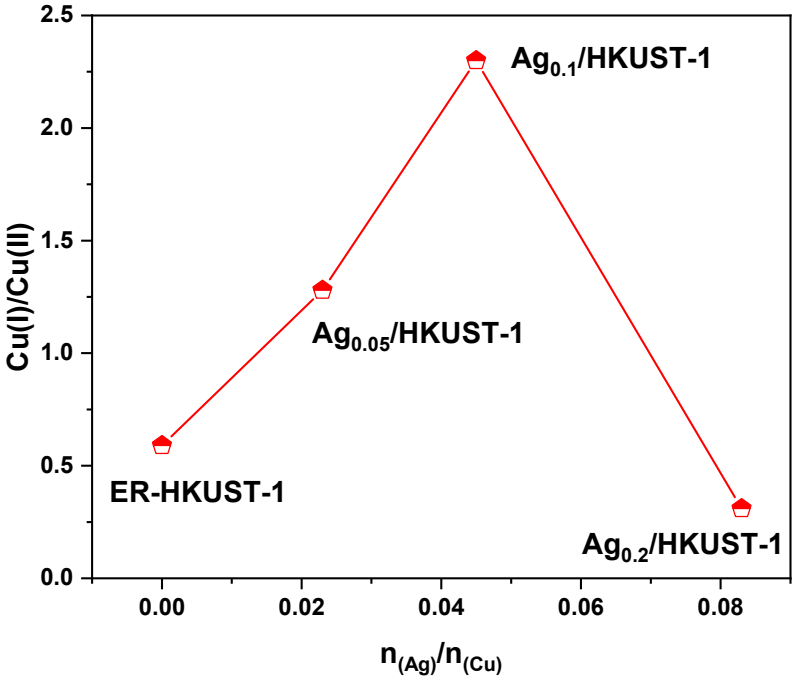

Fig. S8. Cu(I)/Cu(II) molar ratios of ER-HKUST-1, $Ag_{0.05}$/HKUST-1, $Ag_{0.1}$/HKUST-1 and $Ag_{0.2}$/HKUST-1. The Ag/Cu molar ratios of the samples were obtained from ICP-ES measurements and Cu(I)/Cu(II) molar ratios from the integration of Cu $2p_{3/2}$ XPS peaks.

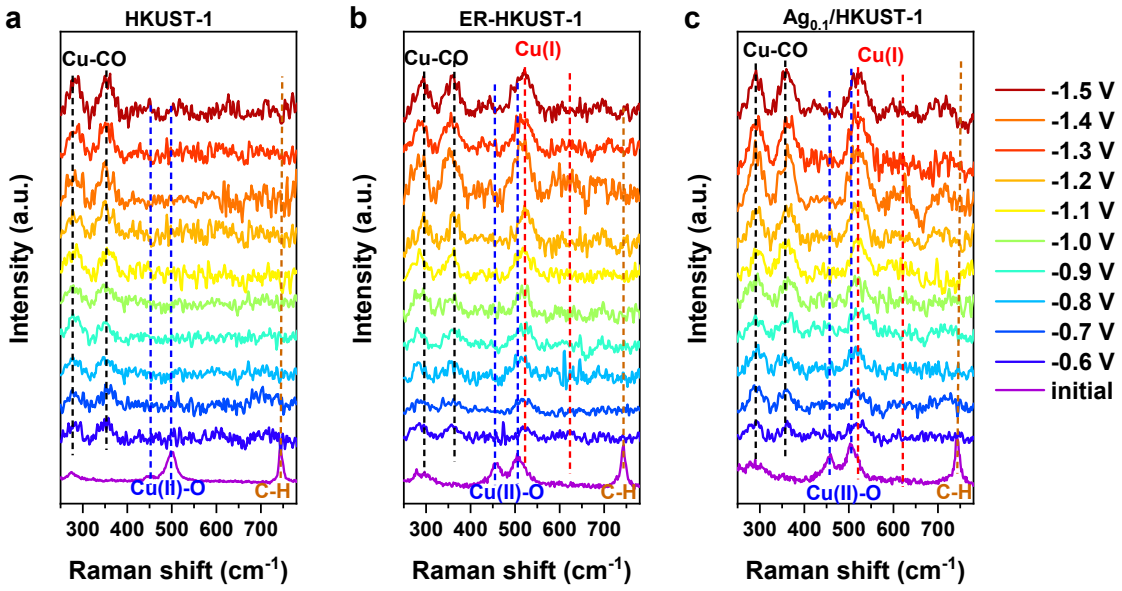

Fig. S9. *In situ* Raman spectra during electrochemical reconstruction under different potential of (a) HKUST-1, (b) ER-HKUST-1 and (c) $Ag_{0.1}$/HKUST-1. *In situ* Raman measurements were carried out using a laser confocal Raman microspectrometer (Horiba HR-800) with a 532 nm laser. The experiments were conducted in a custom-designed three electrode SERS cell with an Ag/AgCl electrode as the reference electrode and a graphite rod as the counter electrode in the anode chamber. The electrolyte was 1.0 M KOH plugged with CO_2.

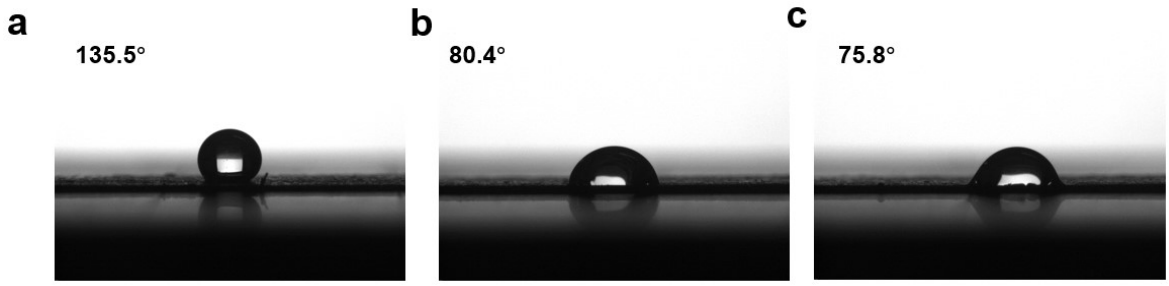

Fig. S10. The average water droplet contact angle of (a) $Ag_{0.1}$/HKUST-1, (b) ER-HKUST-1 and (c) HKUST-1 after reconstruction.

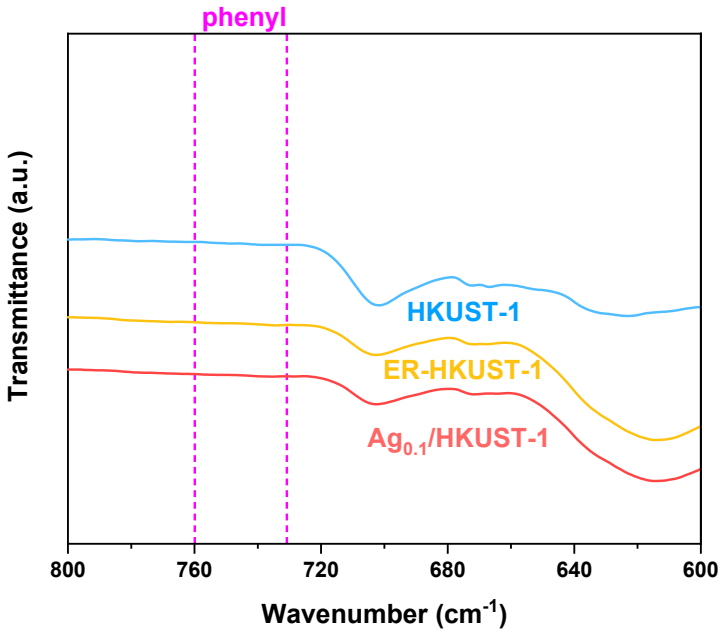

Fig. S11. FT-IR spectra of HKUST-1, ER-HKUST-1 and $Ag_{0.1}$/HKUST-1 after reconstruction.

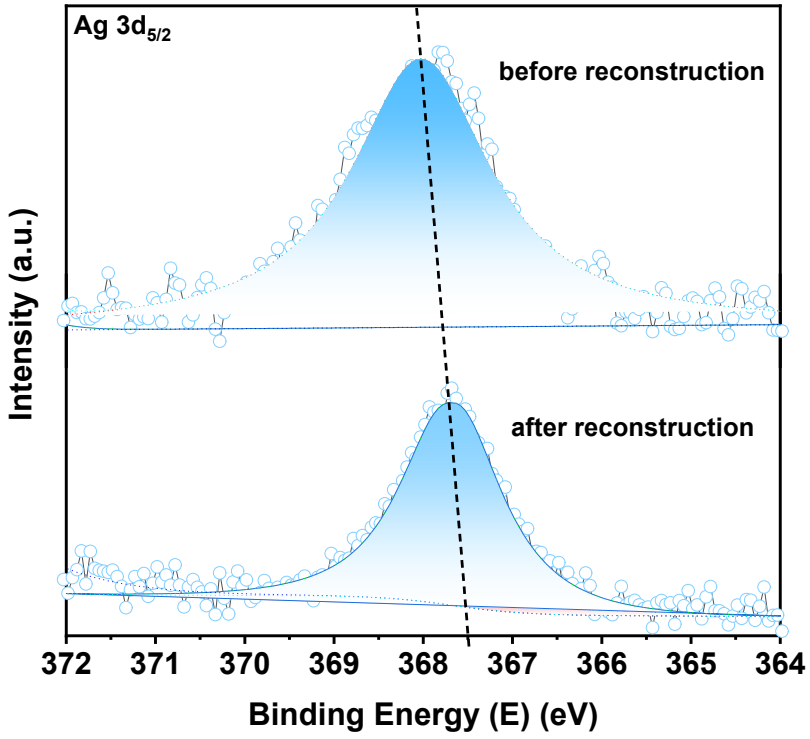

Fig. S12. High-resolution Ag $3d_{5/2}$ XPS profiles of Ag/Cu/$Cu_2O_{Ag0.1/HKUST-1}$ before and after reconstruction.

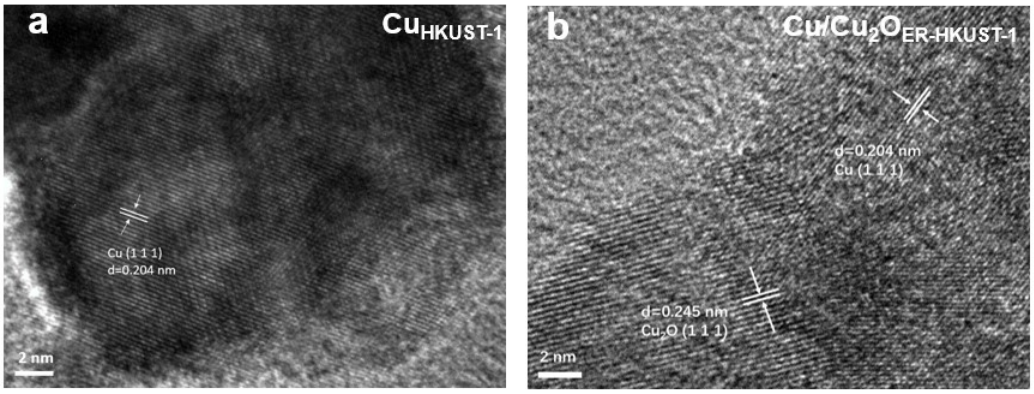

Fig. S13. HRTEM images of (a) $Cu_{HKUST-1}$ and (b) $Cu/Cu_2O_{ER-HKUST-1}$.

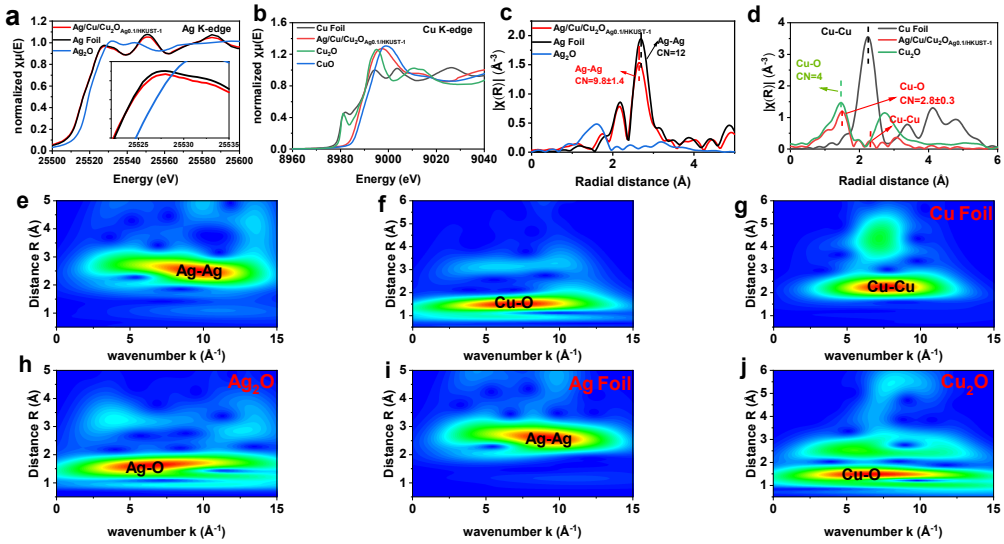

Fig. S14. (a) Normalized XANES and the enlarged white line (the inset) spectra of Ag K-edge in $Ag/Cu/Cu_2O_{Ag0.1HKUST-1}$, Ag_2O and Ag Foil. (b) Normalized XANES of Cu K-edge in $Ag/Cu/Cu_2O_{Ag0.1HKUST-1}$, Cu_2O, CuO and Cu Foil. (c) Fourier transform of Ag K-edge in $Ag/Cu/Cu_2O_{Ag0.1HKUST-1}$, Ag_2O and Ag Foil. (d) Fourier transform of Cu K-edge in $Ag/Cu/Cu_2O_{Ag0.1HKUST-1}$, Cu_2O and Cu Foil. Wavelet transform of (e) Ag and (f) Cu K-edges in $Ag/Cu/Cu_2O_{Ag0.1HKUST-1}$. Wavelet transform of (g) Cu foil, (h) Ag_2O, (i) Ag Foil and (j) Cu_2O.

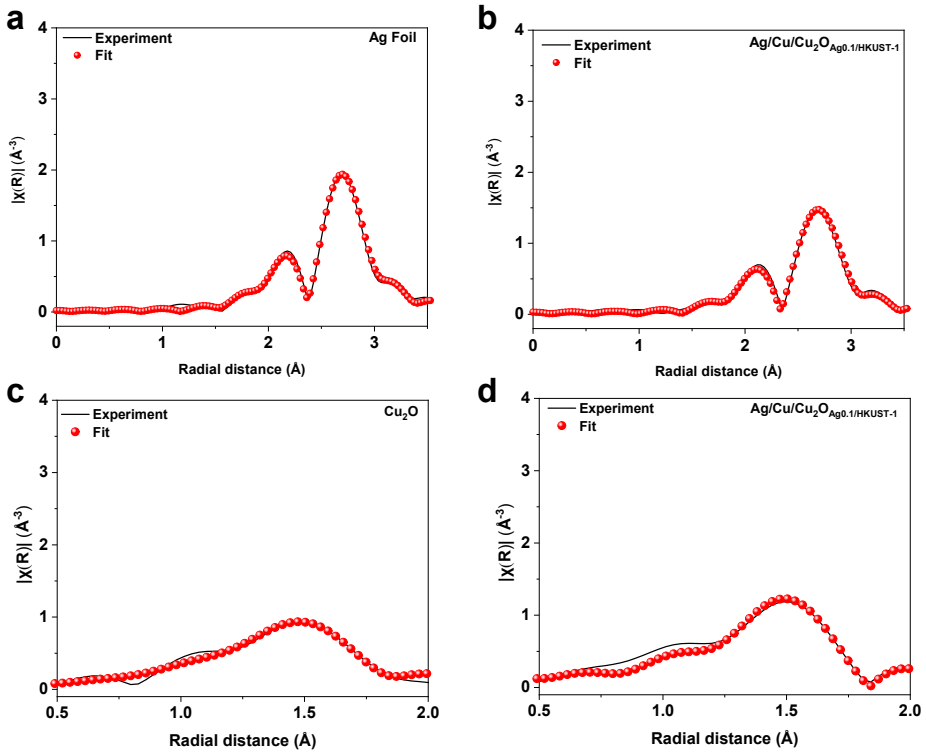

Fig. S15. Fourier transform of Ag K-edge EXAFS fitting results of (a) Ag foil and (b) $Ag/Cu/Cu_2O_{Ag0.1HKUST-1}$, and Cu K-edge EXAFS fitting results of (c) Cu_2O and (d) $Ag/Cu/Cu_2O_{Ag0.1HKUST-1}$.

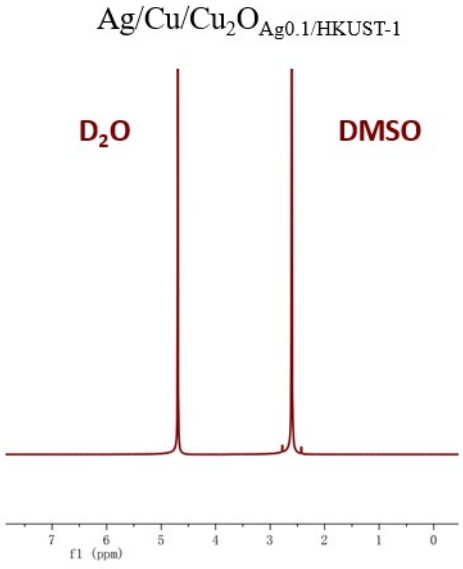

Fig. S16. ^1H NMR of liquid products obtained on $Ag/Cu/Cu_2O_{Ag0.1/HKUST-1}$ at -1.3 V (vs. RHE) in Flow cell. 0.1 mL of the electrolyte was mixed with 0.5 mL of D_2O, and DMSO (Dimethyl sulphoxide) was used as an internal standard.

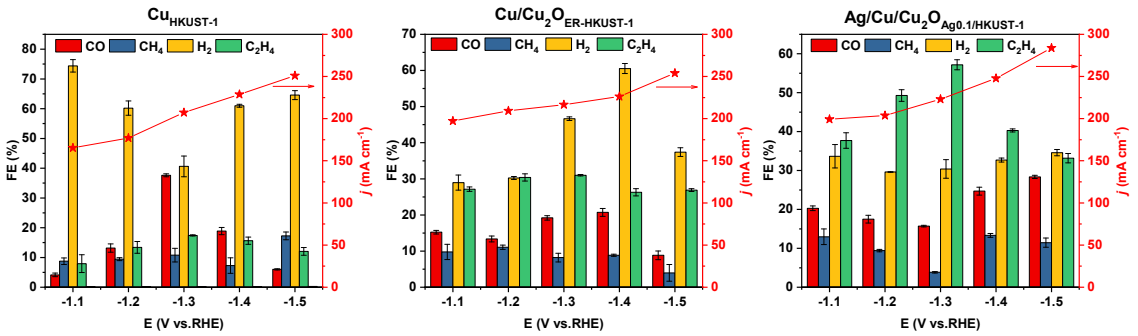

Fig. S17. The FE of all products and the corresponding current density for $Cu_{HKUST-1}$, $Cu/Cu_2O_{ER-HKUST-1}$ and $Ag/Cu/Cu_2O_{Ag0.1/HKUST-1}$.

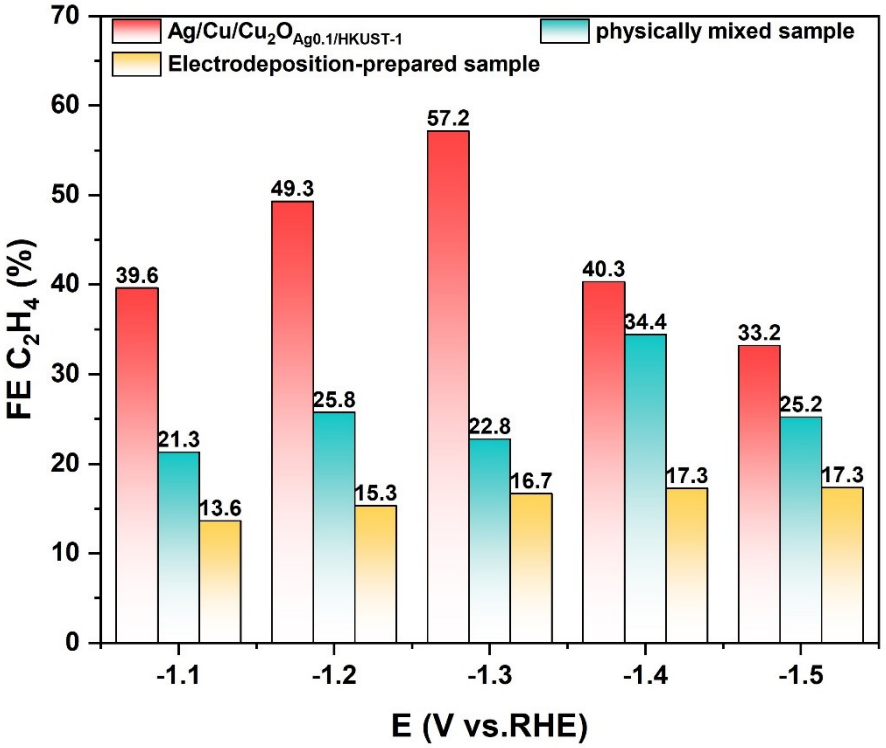

Fig. S18. FEs of C_2H_4 on $Ag/Cu/Cu_2O_{Ag0.1/HKUST-1}$, physically mixed sample and electrodeposition-prepared sample at various working potentials.

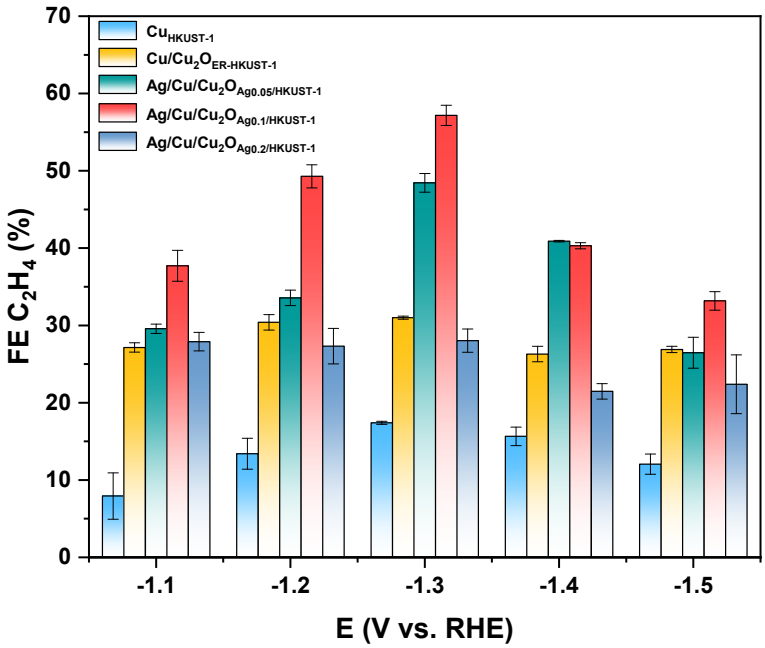

Fig. S19. FE for C_2H_4 at different applied potentials of HKUST-1, ER-HKUST-1, $Ag/Cu/Cu_2O_{Ag0.05/HKUST-1}$, $Ag/Cu/Cu_2O_{Ag0.1/HKUST-1}$ and $Ag/Cu/Cu_2O_{Ag0.2/HKUST-1}$.

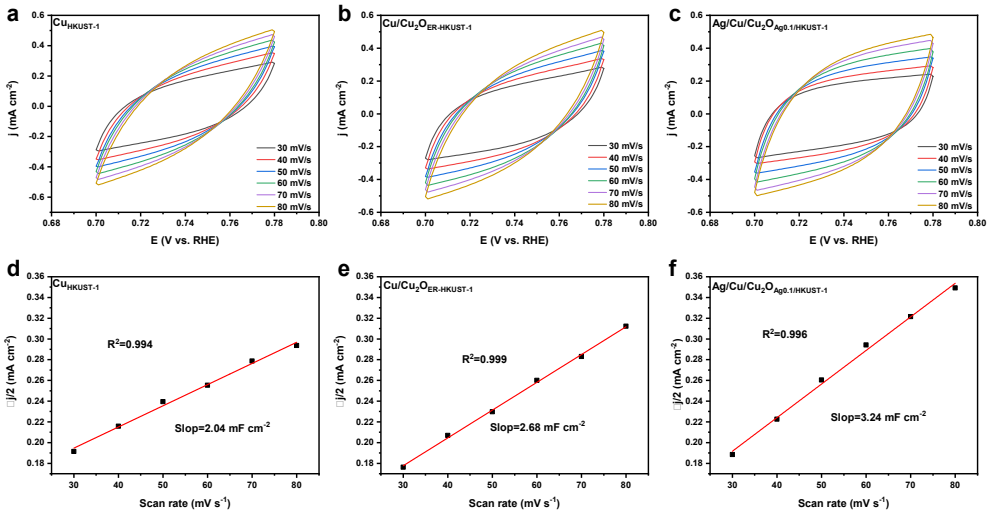

Fig. S20. (a-c) CVs with various scan rates of $Cu_{HKUST-1}$, $Cu/Cu_2O_{ER-HKUST-1}$ and $Ag/Cu/Cu_2O_{Ag0.1/HKUST-1}$. (d-f) Current due to double-layer charging plotted against scan rates of $Cu_{HKUST-1}$, $Cu/Cu_2O_{ER-HKUST-1}$ and $Ag/Cu/Cu_2O_{Ag0.1/HKUST-1}$.

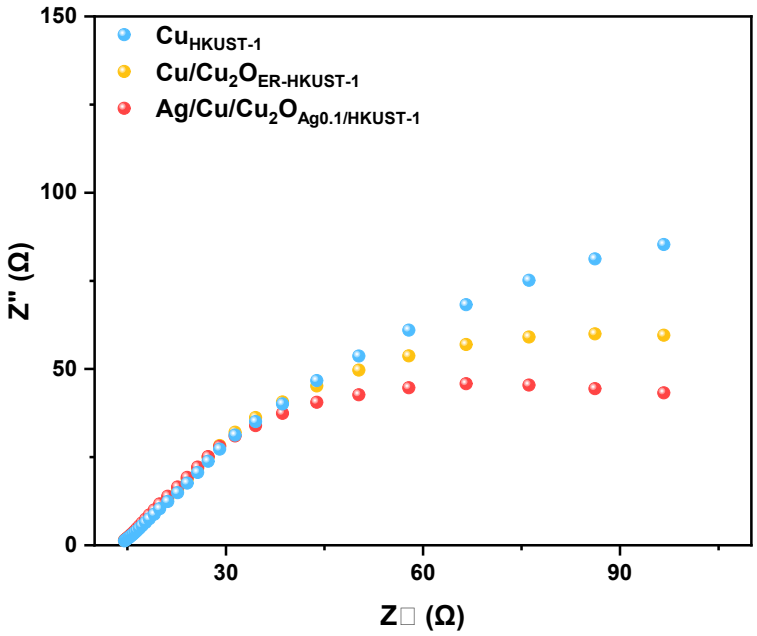

Fig. S21. EIS spectra of $Cu_{HKUST-1}$, $Cu/Cu_2O_{ER-HKUST-1}$ and $Ag/Cu/Cu_2O_{Ag0.1/HKUST-1}$ at -1.0 V vs. RHE for CO_2RR.

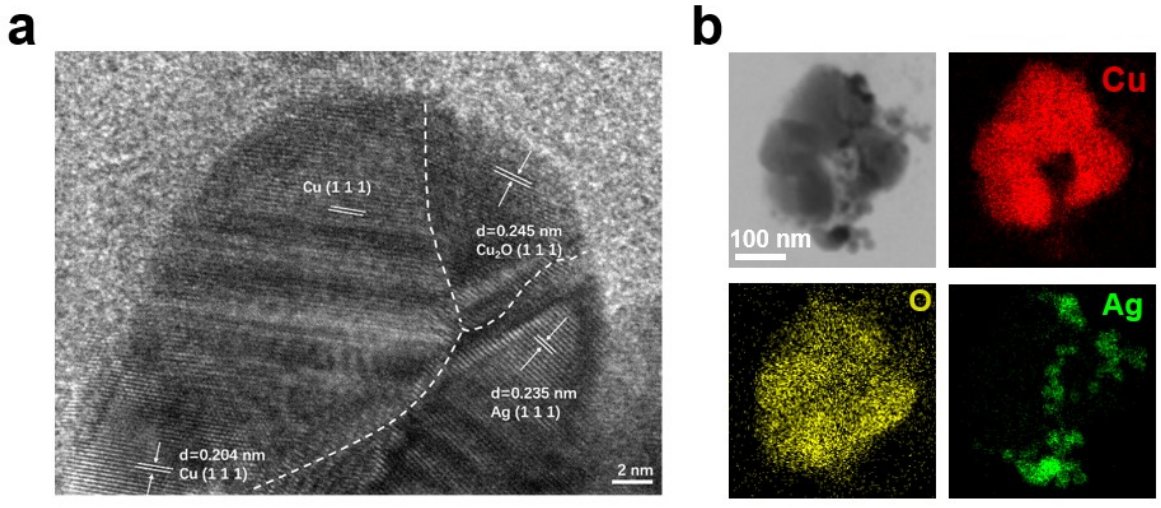

Fig. S22. (a) HR-TEM image and (b) elemental mapping of $Ag/Cu/Cu_2O_{Ag0.1/HKUST-1}$ after CO_2RR test.

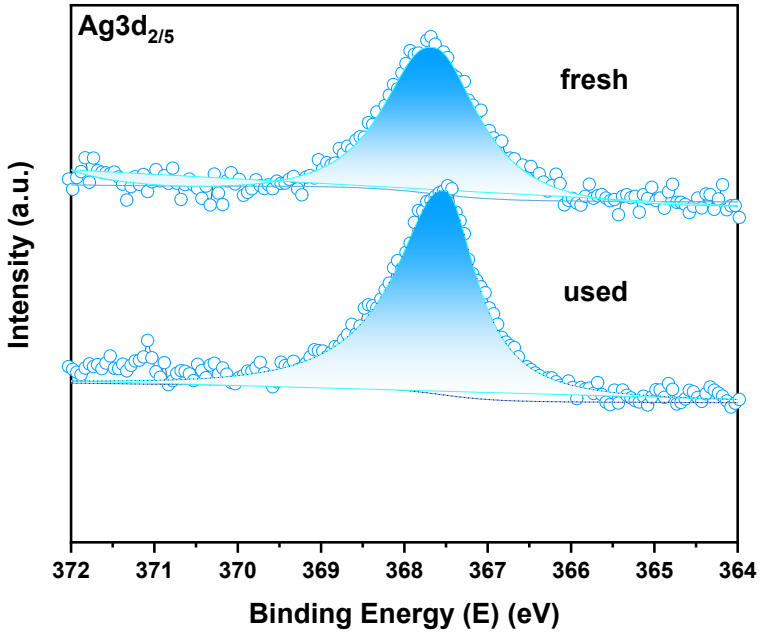

Fig. S23. High-resolution Ag $3d_{5/2}$ XPS profile of Ag/Cu/$Cu_2O_{Ag0.1/HKUST-1}$ before and after CO_2RR test.

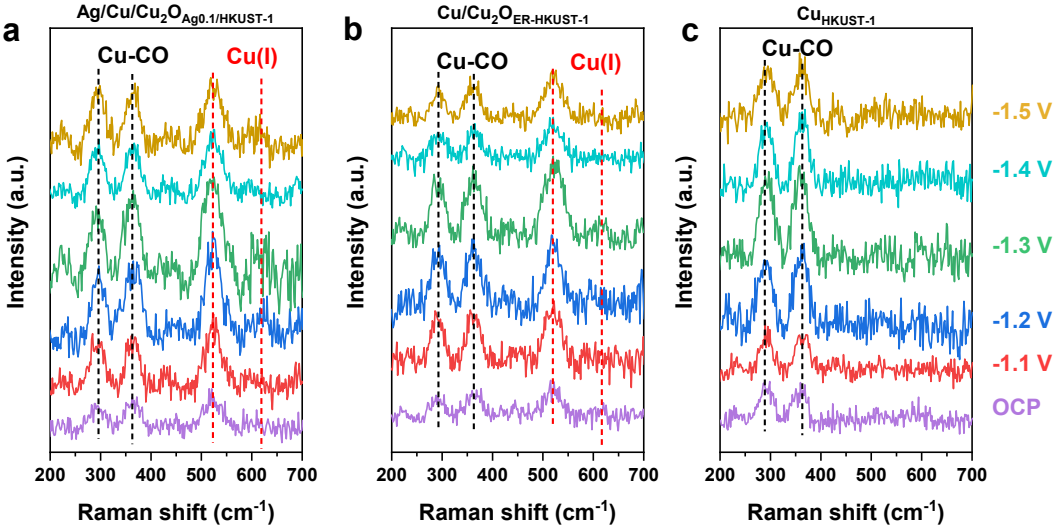

Fig. S24. *In situ* Raman spectra of (a) Ag/Cu/$Cu_2O_{Ag0.1/HKUST-1}$HKUST-1, (b) Cu/$Cu_2O_{ER-HKUST-1}$ and (c) $Cu_{HKUST-1}$ collected at different potentials during CO_2RR.

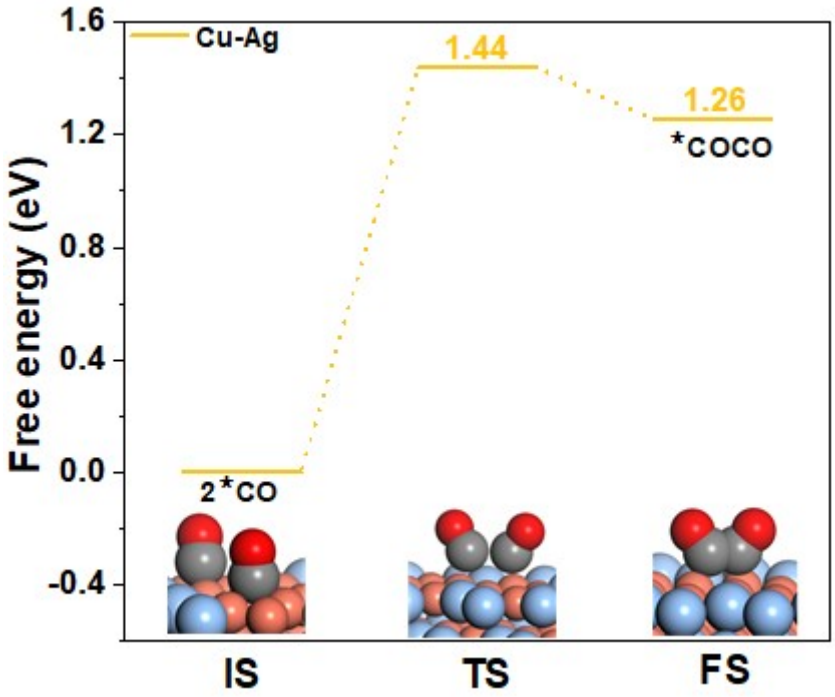

Fig. S25. Energy profiles for initial state (IS), transition state (TS) and final states (FS) of *CO-*CO coupling on a Cu-Ag model.

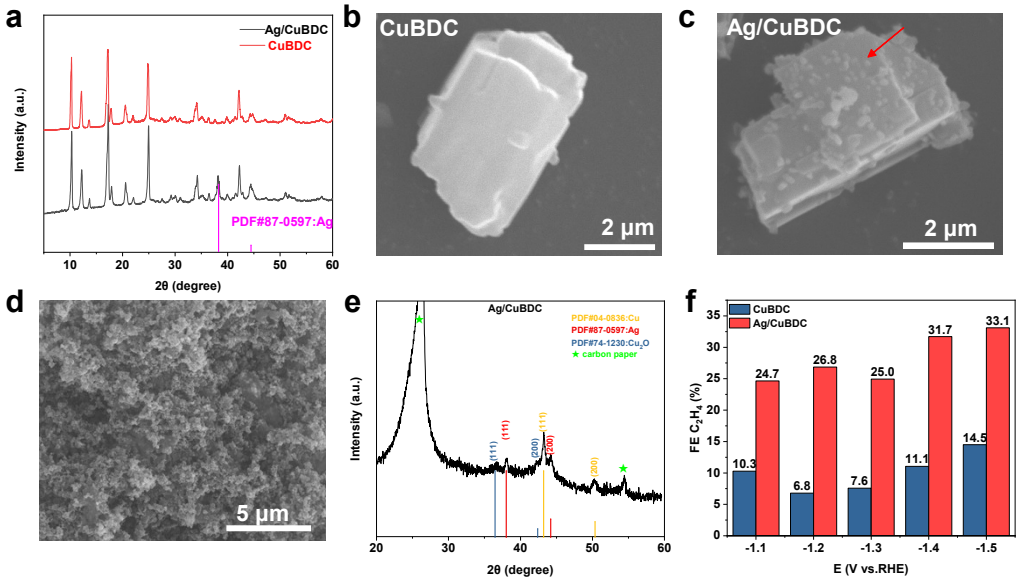

Fig. S26. (a) XRD patterns and (b and c) SEM images of CuBDC and Ag/CuBDC. (d) SEM image and (e) XRD pattern of Ag/CuBDC after reconstruction. (f) FE of C_2H_4 on the reconstructed CuBDC and Ag/CuBDC at different applied potentials.

Synthesis of CuBDC: $Cu(NO_3)_2 \cdot 3H_2O$ (0.50 g) was completely dissolved in 30 mL DMF, and then H_2BDC (0.34 g) was added into the above solution with continuous

stirring for 5 h at 100 °C. The precipitates were centrifuged, washed with DMF and dried in a vacuum oven at 60 °C overnight.

Synthesis of Ag/CuBDC: $AgNO_3$ was dissolved in 20 mL hydroalcoholic solution (V_{DMF} : V_{EtOH}: V_{H2O} = 10:9:1), and then the as-prepared CuBDC was added into the above solution with continuous stirring for 20 h at 85 °C. The precipitates were centrifuged, washed with DMF and dried in a vacuum oven at 60 °C overnight.

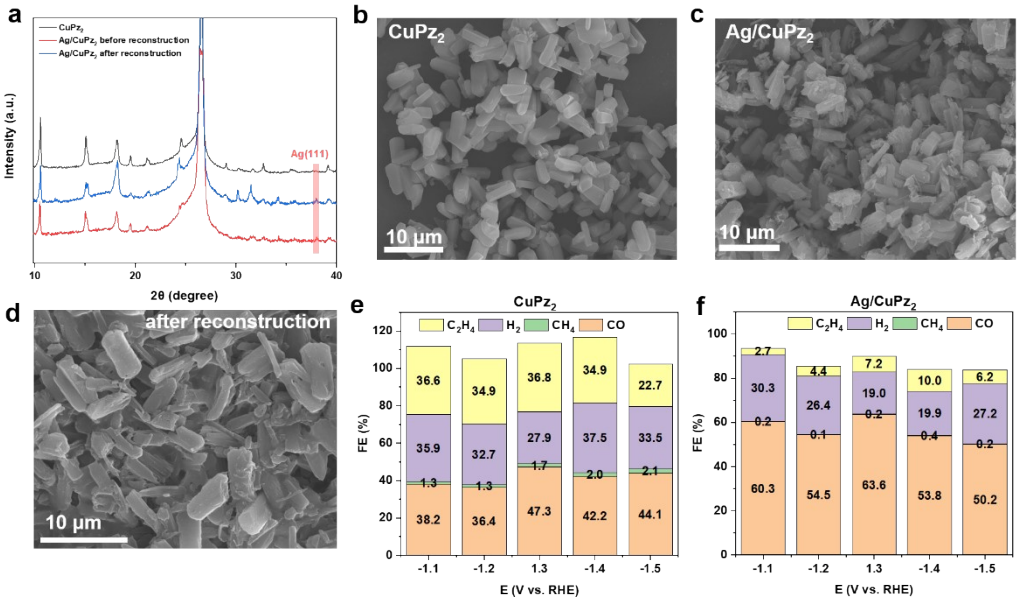

Fig. S27. (a) XRD patterns and (b-d) SEM images of $CuPz_2$, $Ag/CuPz_2$ and reconstructed $Ag/CuPz_2$. FE of C_2H_4 at different applied potentials on (e) $CuPz_2$ and (f) $Ag/CuPz_2$.

Synthesis of $CuPz_2$: $CuPz_2$ was synthesized according to the reported literature with small modifications.[1] First, $Cu(NO_3)_2{\cdot}3H_2O$ (1.691 g, 7 mmol) was completely dissolved in 40 mL of 28% concentrated ammonia solution, and then pyrazole (1.021 g, 15 mmol) was completely dissolved in 40 mL of 28% concentrated ammonia solution. Under vigorous stirring, the two solutions were mixed. The obtained dark blue suspension was stirred for 20 minutes to obtain a blue precipitate. The precipitate was filtered, washed several times with 28% concentrated ammonia and ultrapure water, and then dried overnight in a vacuum oven at 60 °C.

Synthesis of Ag/$CuPz_2$: $AgNO_3$ was dissolved in 10 mL of hydroalcoholic solution (V_{EtOH}: V_{H2O} = 9:1), and then the as-prepared $CuPz_2$ was added into the above solution with continuous stirring for 20 h at 85 °C. The precipitates were centrifuged, washed with ethanol and dried in a vacuum oven at 60 °C overnight.

Table S1. EXAFS fitting results

Sample	Scattering path	Distance (Å)	C.N.	σ^2	$\triangle E_0$ (eV)	R-factor
Ag Foil	Ag-Ag	2.87	12	0.009	2.50±0.36	0.007
$Ag/Cu/Cu_2O_{Ag0.1HKUST-1}$	Ag-Ag	2.86	9.8±1.4	0.009	1.48±0.88	0.006
Cu_2O	Cu-O	1.92	4	0.005	-0.56±1.97	0.011
$Ag/Cu/Cu_2O_{Ag0.1HKUST-1}$	Cu-O	1.94	2.8±0.3	0.001	-1.09±1.41	0.009

Note: In Ag-Ag path S_0^2 (0.971) was determined by Ag foil. In Cu-O path S_0^2 (0.728) was determined by Cu_2O.

Table S2. Electrochemical CO_2RR Performance of Cu-based electrocatalysts toward C_2H_4.

Entry	Materials	*j* (mA cm^{-2})	stability	FE of C_2H_4	Cell	Refs.
This work	**$Ag_{0.1}$/HKUST-1**	**220**	**10h**	**57.2%**	**flow cell**	**This work**
1	S-HKUST-1	150	8h	50%	flow cell	[2]
2	$CuPz_2$-Act-30	15	12h	70.2 ± 1.7%	H-cell	[1]
3	Cu dimer distorted HKUST-1	262	2.3h	45%	flow cell	[3]
4	Cu−N−C-800	27.6	10h	24.8%	H-cell	[4]
5	Cutrz	280	6h	50%	flow cell	[5]
6	MAF-2E	10.9	8h	51.2 ± 2.3%	H-cell	[6]
7	NNU-33(H)	176.08	5h	27.71%	flow cell	[7]
8	Cu-ade MOF	8.5	8h	45%	H-cell	[8]
9	Cu−DBC	203	2.5h	~4%	flow cell	[9]
10	Cu_2O@CuHHTP	14.8	5h	~5%	H-cell	[10]
11	PorCu	48	1h	~17%	H-cell	[11]
12	CPFs	10.2	2h	18%	H-cell	[12]
13	AuNN@PCN-222(Cu)	~10	10h	52.5%	H-cell	[13]
14	PcCu−Cu−O	7.3	4h	50%	H-cell	[14]
15	CuPc	11.2	2.8h	25%	H-cell	[15]
16	Co-doped $Cu_2(BDC)_2$	282	3h	15.6%	flow cell	[16]
17	BEN–Cu–BTC	7	8h	11.2%	H-cell	[17]
18	Cu-CPW	13.2	5h	20%	H-cell	[18]
19	2F-Cu-BDC	150	3h	40%	flow cell	[19]
20	Cu nanoribbons.	200	10h	42%	flow cell	[20]
21	Cu-PzH	346	3.8h	60%	flow cell	[21]
22	e-Pb/Cu_2O-3.4%	203.8	10h	~33%	flow cell	[22]
23	Cu_2O@SiO_2–NH_2	280	15h	35%	flow cell	[23]
24	ZrO_2/Cu–Cu_2O	24	6h	62.5%	H-cell	[24]
25	Ag@Cu_2O-2	100	10h	31.5%	flow cell	[25]
26	Cu_2O-BN	~40	14h	15%	H-cell	[26]

REFERENCES

[1] C. Liu, X.-D. Zhang, J.-M. Huang, M.-X. Guan, M. Xu and Z.-Y. Gu, *ACS Catalysis* **2022**, *12*, 15230-15240.

[2] C. F. Wen, M. Zhou, P. F. Liu, Y. Liu, X. Wu, F. Mao, S. Dai, B. Xu, X. L. Wang, Z. Jiang, P. Hu, S. Yang, H. F. Wang and H. G. Yang, *Angewandte Chemie-International Edition* **2022**, *61*, e202111700.

[3] N. Dae-Hyun, O. S. Bushuyev, J. Li, P. De Luna, A. Seifitokaldani, D. Cao-Thang, F. P. G. de Arquer, Y. Wang, Z. Liang, A. H. Proppe, C. S. Tan, P. Todorovic, O. Shekhah, C. M. Gabardo, J. W. Jo, J. Choi, M.-J. Choi, S.-W. Baek, J. Kim, D. Sinton, S. O. Kelley, M. Eddaoudi and E. H. Sargent, *Journal of the American Chemical Society* **2018**, *140*, 11378-11386.

[4] A. Guan, Z. Chen, Y. Quan, C. Peng, Z. Wang, T.-K. Sham, C. Yang, Y. Ji, L. Qian, X. Xu and G. Zheng, *ACS Energy Letters* **2020**, *5*, 1044-1053.

[5] D.-S. Huang, H.-L. Zhu, Z.-H. Zhao, J.-R. Huang, P.-Q. Liao and X.-M. Chen, *ACS Catalysis* **2022**, *12*, 8444-8450.

[6] L.-L. Zhuo, P. Chen, K. Zheng, X.-W. Zhang, J.-X. Wu, D.-Y. Lin, S.-Y. Liu, Z.-S. Wang, J.-Y. Liu, D.-D. Zhou and J.-P. Zhang, *Angewandte Chemie-International Edition* **2022**, *61*, e202204967.

[7] L. Zhang, X.-X. Li, Z.-L. Lang, Y. Liu, J. Liu, L. Yuan, W.-Y. Lu, Y.-S. Xia, L.-Z. Dong, D.-Q. Yuan and Y.-Q. Lan, *Journal of the American Chemical Society* **2021**, *143*, 3808-3816.

[8] F. Yang, A. Chen, P. L. Deng, Y. Zhou, Z. Shahid, H. Liu and B. Y. Xia, *Chemical Science* **2019**, *10*, 7975-7981.

[9] Y. Zhang, L.-Z. Dong, S. Li, X. Huang, J.-N. Chang, J.-H. Wang, J. Zhou, S.-L. Li and Y.-Q. Lan, *Nature Communications* **2021**, *12*, 6390.

[10] J.-D. Yi, R. Xie, Z.-L. Xie, G.-L. Chai, T.-F. Liu, R.-P. Chen, Y.-B. Huang and R. Cao, *Angewandte Chemie-International Edition* **2020**, *59*, 23641-23648.

[11] Z. Weng, J. Jiang, Y. Wu, Z. Wu, X. Guo, K. L. Materna, W. Liu, V. S. Batista, G. W. Brudvig and H. Wang, *Journal of the American Chemical Society* **2016**, *138*, 8076-8079.

[12] Y. Zhou, S. Chen, S. Xi, Z. Wang, P. Deng, F. Yang, Y. Han, Y. Pang and B. Y. Xia, *Cell Reports Physical Science* **2020**, *1*.

[13] X. Xie, X. Zhang, M. Xie, L. Xiong, H. Sun, Y. Lu, Q. Mu, M. H. Rummeli, J. Xu, S. Li, J. Zhong, Z. Deng, B. Ma, T. Cheng, W. A. Goddard, III and Y. Peng, *Nature Communications* **2022**, *13*.

[14] X.-F. Qiu, H.-L. Zhu, J.-R. Huang, P.-Q. Liao and X.-M. Chen, *Journal of the American Chemical Society* **2021**, *143*, 7242-7246.

[15] S. Kusama, T. Saito, H. Hashiba, A. Sakai and S. Yotsuhashi, *ACS Catalysis* **2017**, *7*, 8382-8385.

[16] B. Kim, Y. C. Tan, Y. Ryu, K. Jang, H. G. Abbas, T. Kang, H. Choi, K.-S. Lee, S. Park, W. Kim, P.-P. Choi, S. Ringe and J. Oh, *ACS Energy Letters* **2023**, *8*, 3356-3364.

[17] Y.-S. Cheng, X.-P. Chu, M. Ling, N. Li, K.-L. Wu, F.-H. Wu, H. Li, G. Yuan and X.-W. Wei, *Catalysis Science & Technology* **2019**, *9*, 5668-5675.

[18] W. Zhang, C. Huang, J. Zhu, Q. Zhou, R. Yu, Y. Wang, P. An, J. Zhang, M. Qiu, L. Zhou, L. Mai, Z. Yi and Y. Yu, *Angewandte Chemie-International Edition* **2022**, *61*, e202112116.

[19] R. Chen, L. Cheng, J. Liu, Y. Wang, W. Ge, C. Xiao, H. Jiang, Y. Li and C. Li, *Small* **2022**, *18*, 2200720.

[20] H. Huo, J. Wang, Q. Fan, Y. Hu and J. Yang, *Advanced Energy Materials* **2021**, *11*, 2102447.

[21] R. Wang, J. Liu, Q. Huang, L.-Z. Dong, S.-L. Li and Y.-Q. Lan, *Angewandte Chemie-International Edition* **2021**, *60*, 19829-19835.

[22] X. Ma, X. Song, L. Zhang, L. Wu, J. Feng, S. Jia, X. Tan, L. Xu, X. Sun and B. Han, *Green Chemistry*

2023, *25*, 7635-7641.
[23] Z.-Y. Zhang, H. Tian, H. Jiao, X. Wang, L. Bian, Y. Liu, N. Khaorapapong, Y. Yamauchi and Z.-L. Wang, *Journal of Materials Chemistry A* **2024**, *12*, 1218-1232.
[24] P. P. Guo, Z. H. He, S. Y. Yang, W. T. Wang, K. Wang, C. C. Li, Y. Y. Wei, Z. T. Liu and B. X. Han, *Green Chemistry* **2022**, *24*, 1527-1533.
[25] F. Yu, X. Liu, L. Liao, G. Xia and H. Wang, *Small* **2023**, *19*.
[26] Y. Zhou, Y. Yao, R. Zhao, X. Wang, Z. Fu, D. Wang, H. Wang, L. Zhao, W. Ni, Z. Yang and Y.-M. Yan, *Angewandte Chemie-International Edition* **2022**, *61*.